

Mechanisms of DNA Hybridization: Transition Path Analysis of a Simulation-Informed Markov Model

Raymond Jin and Lutz Maibaum^{a)}

Department of Chemistry, University of Washington, Seattle, WA 98195

Complementary DNA strands in solution reliably hybridize to form stable duplexes. We study the kinetics of the hybridization process and the mechanisms by which two initially isolated strands come together to form a stable double helix. We adopt a multi-step computational approach. First, we perform a large number of Brownian dynamics simulations of the hybridization process using the coarse-grained oxDNA2 model. Second, we use these simulations to construct a Markov State Model of DNA dynamics that uses a state decomposition based on the inter-strand hydrogen bonding pattern. Third, we take advantage of Transition Path Theory to obtain quantitative information about the thermodynamic and dynamic properties of the hybridization process. We find that while there is a large ensemble of possible hybridization pathways there is a single dominant mechanism in which an initial base pair forms close to either end of the nascent double helix, and the remaining bases forms pairs sequentially in a zipper-like fashion. We also show that the number of formed base pairs by itself is insufficient to describe the transition state of the hybridization process.

INTRODUCTION

Deoxyribonucleic acid (DNA) is a biopolymer that contains the information of life. Its crucial role in biology and its many uses in technological applications such as DNA origami^{1,2} and nanoparticle linker^{3,4} depend on DNA's ability to hybridize: two single-stranded DNA (ssDNA) molecules bind to form a double-stranded DNA (dsDNA) duplex. The duplex is stabilized by hydrogen bonds between the nucleobases adenine (A), thymine (T), guanine (G), and cytosine (C).

The mechanism of hybridization remains a topic of current research. Classically, hybridization is thought of as a two-step process in which the strands first form an initial nucleus of hydrogen-bonded base pairs, which is then followed by the strands "zipping up" to form the fully hybridized double helix⁵. It was later found that at least three base pairs were necessary for a thermodynamically stable binding nucleus⁶. Recent experiments on RNA, on the other hand, found a threshold of seven base pairs⁷. A more complex mechanism based on a three-step process has been proposed⁸. Here the two strands initially bind by non-specific interactions. The first stable base pair is then formed either through a one-dimensional sliding motion in which the strands search for an initial nucleation point, or through internal displacements in which the strands traverse each other in an inchworm-like motion. Once an initial nucleation point is found, the bases zip up to fully hybridize as in the classical mechanism.

It is challenging to observe hybridization in a base-by-base manner in experiments. Previous work has been done on detection of hybridization in bulk solution using a variety of techniques, including absorption spectroscopy^{5,9,10}, surface-enhanced Raman spectroscopy¹¹, and electrochemistry¹². Recently, there have been advances in single molecule experiments to study hybridization using electrochemical techniques¹³ and force

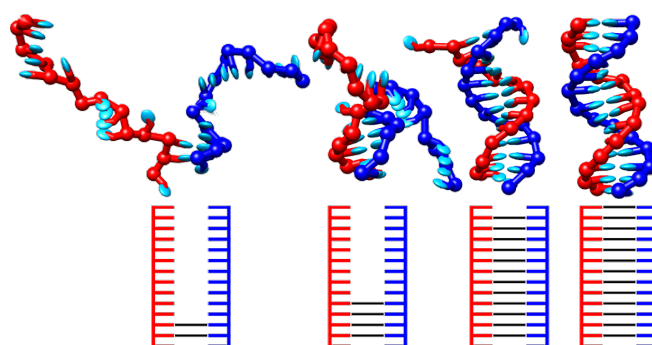


FIG. 1. Top: Snapshots from a typical hybridization trajectory of a coarse-grained oxDNA2 simulation. Each strand has 14 bases, and each base is represented by two particles. The spheroid represents the backbone and the disc represents the base. The two strands make an initial contact near the end of the strand and then zip up to a fully hybridized state. Bottom: Schematic representation of the inter-strand hydrogen bonding pattern. Red and blue lines represent the two strands, and black lines denote hydrogen bonds.

probes^{14,15}. There have also been studies of DNA at the base level using fluorescence resonance energy transfer^{7,16,17} and fluorescence correlation spectroscopy^{18–20}.

Molecular Dynamics (MD) computer simulations can provide insight into the hybridization mechanism on a base-by-base level. While an atomistic description of the two strands, water, and counterions would provide the highest resolution, it is computationally too expensive to obtain a large dataset of hybridization trajectories. Coarse-grained models sacrifice detail for speed, and several such models of DNA can be found in the literature. In this work we use the recently developed oxDNA 2 model, in which each nucleotide is described by three interaction sites: a backbone site, a hydrogen bonding site, and a stacking site (Figure 1 top). It is parametrized to match the melting temperatures of the SantaLucia model²¹ at various salt concentrations, as well as physical characteristics such as major-minor grooving and radius

^{a)}Electronic mail: maibaum@uw.edu

of gyration²². Interactions in the oxDNA2 model include stacking, hydrogen bonding and electrostatics. It has been used to study processes such as hybridization²³ and toehold-mediated strand displacement²⁴. In their study on hybridization, Ouldrige and coworkers used Forward Flux Sampling to guide the system toward the duplexed state²³. They found a mechanism consistent with a two step process of nucleation and zipping up similar to the classical mechanism.

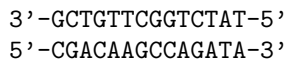
Here we adopt a different approach to obtaining mechanistic information about the hybridization pathway from coarse-grained simulations. Starting with a large set of hybridization trajectories we construct a Markov State Model (MSM) that describes the stochastic dynamics of the system across a large set of discrete states that represent the two strands' hydrogen bonding pattern. The generation of MSMs from MD simulations to describe the dynamics of complex systems has been pioneered in the context of protein folding^{25–28}. Having obtained an MSM, we use the framework of Transition Path Theory (TPT)²⁹ to obtain quantitative information about the ensemble of pathways by which DNA hybridizes.

METHODS

oxDNA

We use the coarse grained oxDNA2 model to simulate DNA hybridization²². oxDNA2 includes implicit solvent and each base is represented by three particles. One particle represents the backbone, and the other two particles represent the nucleobase. oxDNA2 was parameterized to match the melting temperatures of the SantaLucia model^{21,22}. An important difference in oxDNA2 from physical DNA is the hydrogen bonding interaction. In oxDNA, only bases which are complementary contribute to the hydrogen bonding energy. Hydrogen bonding between non-Watson Crick pairs is ignored. Another difference in the oxDNA2 model is the hydrogen bond interaction energy between A-T and G-C is the same while physical G-C hydrogen bonds are stronger due to the additional hydrogen bond.

We simulated two strands of single stranded DNA with $N = 14$ bases each. The sequences are



These strands are complimentary and designed to limit non-intended base-pairing²³. The strands had a random starting configuration and were allowed to simulate for 3 μ s or until the strands had fully hybridized. Temperature was held at 300 K using a Andersen thermostat with the time between collisions of 103 steps and the probability of collision is 0.02 as done in previous work²³. The effective salt concentration was 0.5 M. Strands were placed in a cubic box of side length 10nm. The simulation timestep was 15fs. Strands were determined to be fully hybridized

when all bases had hydrogen bonds with their native pair. Two bases were considered hydrogen bonded if their hydrogen bond contribution to the interaction energy was larger than 1.79 kcal/mol.

Markov State Model

In order to create an MSM, we partitioned the raw molecular dynamics data into individual states at each timestep. The states were partitioned based on the hydrogen bonding pattern of the two strands. The bases on each strand were labelled $i, j = 1 \dots N$ from the 3' end to 5' end. At each timestep, we determined which bases are hydrogen bonded with which other bases. The hydrogen bonding pattern only includes bonding between the two strands; instances of intrastrand bonding were ignored. If a base hydrogen bonds with more than one other base, the strongest bond was the only one to be recorded. From the list of hydrogen bonds, we labelled each state s with a number m which encoded the hydrogen bond sequence,

$$m(s) = \sum_{i=1}^N (N+1)^i \sum_{j=1}^N j \omega_{1ij}(s) \quad (1)$$

where

$$\omega_{\alpha ij}(s) = \begin{cases} 1 & \text{if base } i \text{ in strand } \alpha \text{ is bound to} \\ & \text{base } j \text{ in strand } 3 - \alpha \\ 0 & \text{otherwise} \end{cases} \quad (2)$$

This encoding ensures each state label is unique and we can recover the bonding pattern from the number m . The states s are arbitrarily labelled from 1 to M , the total number of states. State $s = 1$ is the unbound state and states $s = 2 \dots M$ are all states that have hydrogen bonding between the strands.

The Net Binding Count, $C(s)$ of each state is calculated by the difference between the number of bases paired in their native configuration and the number of bases paired in a non-native configuration,

$$C(s) = \sum_{i=1}^N 2\omega_{1i(N+1-i)}(s) - \sum_{j=1}^N \omega_{1ij}(s) \quad (3)$$

where native base pairs are those that would occur in the fully hybridized state. This number can range from $-N \dots N$. When $C(s) = N$ then the system is fully hybridized.

To differentiate between states with more binding at the 3' end or at the 5' end, we create a parameter D , the center of hybridization, which is given by,

$$D(s) = \sum_{i=1}^N h_{1i}(s) \left(\frac{N+1}{2} - i \right) \quad (4)$$

where

$$h_{\alpha i}(s) = \sum_{j=1}^N \omega_{\alpha ij}(s) \quad (5)$$

is one if base i is hydrogen bonded to any base on the other strand, and zero otherwise. States with more positive D have more bonding on strand 1 on the 3' end. States with more negative D have more bonding on strand 1 on the 5' end.

To generate the MSMs we use the MSMBuilder software package³⁰. The model was built from the trajectories using a sliding window and Maximum Likelihood Estimator³¹. Briefly, within each trajectory, we count the number of transitions between states m , which are defined by the hydrogen bonding pattern (Equation 1). A transition is counted $x(t) \rightarrow x(t + \tau)$, where t is an arbitrary time and τ is the lag time. If a sliding window is not used, the only transitions counted would be at multiples of τ (i.e. $x(0) \rightarrow x(\tau) \rightarrow x(2\tau)$). When using a sliding window, the transitions are counted at each timestep (i.e. $x(0) \rightarrow x(\tau), x(1) \rightarrow x(1 + \tau)$)³⁰. For our model, we used a sliding window to generate the count matrix.

The transition probability matrix was estimated from the count matrix using a maximum probability estimator that ensured a reversible transition probability matrix and satisfied detailed balance³¹. Once the transition probability matrix is calculated, we solve the eigenvalue equation,

$$\psi_i T = \lambda_i \psi_i \quad (6)$$

where T is the transition probability matrix, ψ_i is i -th left eigenvector and λ_i is the i -th unique eigenvalue. The λ_i take on values of $|\lambda_i| \leq 1$. The eigenvector with $\lambda_i = 1$ is the equilibrium population. Eigenvectors with $\lambda_i < 1$ represent changes in probability of each of the states. The eigenvalues of these eigenvectors are related to the timescale, t_i , of the change in probability:

$$t_i = -\frac{\tau}{\ln \lambda_i} \quad (7)$$

An important variable of building an MSM is the lag time because smaller lag times create MSMs that do not represent the underlying dynamics because the underlying system is not Markovian at that lag time. However, longer lag times lose information about quicker processes. In order to pick a lag time to create an MSM that accurately represents the underlying system, while keeping as much of the data as possible, we build many MSMs with different lag times τ . For each different lag time, we calculate the 10 longest timescales. As the lag time becomes larger, the timescales should not change anymore which indicates Markovian behavior in the underlying system³¹. Then we choose the lag time at which the plateau starts as the lag time for the rest of the analysis to balance Markovinity and detail.

Transition Path Theory

To determine the important states and mechanisms of hybridization we used Transition Path Theory (TPT) to

analyze the MSM^{26,29,32}. We used it to investigate how a system evolves from state(s) A to state(s) B. In our system, state A is the completely unhybridized state and state B is the fully hybridized state. All other states are considered intermediate states, I. Using TPT, we calculate the forward committor, q^+ , which is the probability of reaching state A before reaching state B. A state in A has a committor of 0 and a state in B has a committor of 1 and states with a committor of 0.5 are transition states. The committor is a measure of how close each state is to the hybridized state and is calculated through a system of equations.

$$-q_i^+ + \sum_{j \in I} T_{ij} q_j^+ = - \sum_{j \in B} T_{ij} \quad (8)$$

For a transition matrix that follows detailed balance, the backwards committor is calculated by $q^- = 1 - q^+$.

We investigate the mechanism using TPT by calculating the most likely paths. The likely paths are those that contain the most flux, which is the expected number of transitions between two states within one timestep. We are only interested in transitions in reactive trajectories. The amount of flux in a reactive path between two states i and j is

$$f_{ij} = \pi_i q_i^- T_{ij} q_j^+ \quad (9)$$

where π is the equilibrium population of a state. Simulations often go back and forth between two states which builds up flux between the two states but is not productive to reaching states in B. We use the net flux to determine path strengths. The net flux removes the effect of going back and forth, and is defined as

$$f_{ij}^+ = \max(f_{ij} - f_{ji}, 0) \quad (10)$$

Paths are found using Dijkstra's algorithm with path strength removed by subtraction to find the next most probable path³³. Another property of states we calculated was the fraction visited for each state. The fraction visited is the fraction of times, going from state A to state B, a particular state is visited³⁴.

One way we calculate rate information is through the mean first passage time of hybridization by the following equation:

$$(I - T')\mathbf{b} = \mathbf{c} \quad (11)$$

$$T' = \begin{cases} T'_{ij} = 2, & \text{if } i \in B \text{ and } j = i \\ T'_{ij} = 0, & \text{if } i \in B \text{ and } j \neq i \\ T'_{ij} = T_{ij}, & \text{otherwise} \end{cases} \quad (12)$$

where I is an $M \times M$ identity matrix, T' is a modified transition matrix as given by equation 12, $\tau \mathbf{b}$ are the mean first passage times, \mathbf{c} is an M -length column vector of all ones except at the sink states which are 0, and B is the set of sink states. The single sink state in our system is the fully hybridized state.

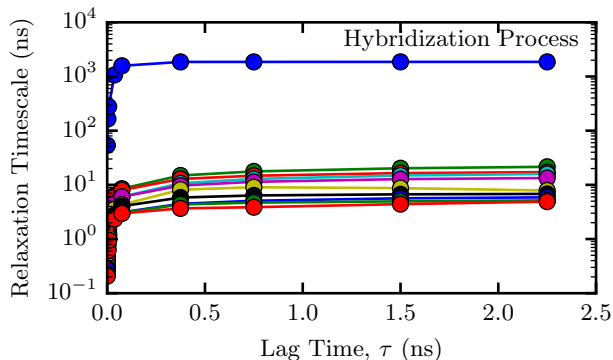


FIG. 2. The ten longest relaxation time scales of MSMs built with increasing lag time τ . Only at sufficiently long lag times the relaxation time scales become independent of τ , which is a necessary condition for the system dynamics to be Markovian. The process with the longest relaxation time scale corresponds to the transition from the fully unbound to a hybridized state (Table I).

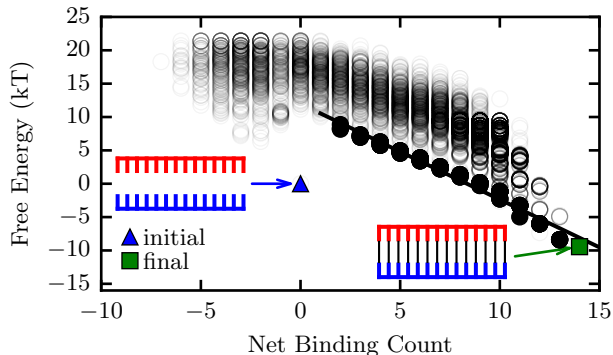


FIG. 3. Free energy of each state, projected onto the Net Binding Count C . The free energy was calculated from the equilibrium probability distribution. Areas with more states appear darker. States with a large number of bound bases tend to have a low free energy. The filled points are the states that appear in the 20 most likely paths. The solid black line is the line of best fit of the filled points.

Another way to calculate the rate of hybridization is through the flux,

$$t_{A \rightarrow B} = \frac{\sum_{i=1}^M \pi_i q_i^-}{\sum_{j=2}^M \pi_1 T_{1j} q_j^+}. \quad (13)$$

RESULTS

To ensure Markovinity, we built a variety of MSMs with differing lag times and calculated the timescales of

State	Element in the Longest Timescale Eigenvector
	-1.00
	0.46
	0.16
	0.16
	0.05

TABLE I. Five states with the largest (by magnitude) values in the eigenvector with the longest relaxation time scale. The eigenvector is normalized so that the unbound state has a value of -1. This relaxation process shifts probability from the unbound state to the completely hybridized and three mostly hybridized states.

the 10 longest relaxation processes. As the lag time increases, we see these timescales start to plateau, indicating the underlying molecular dynamics system is Markovian at the increased lag time (Figure 2). We balance the need for Markovinity and temporal resolution by choosing the smallest lag time that is plateaued. This value is 0.75 nanoseconds. From these timescales, we also see one much longer relaxation process and many shorter relaxation processes. This long timescale process is important because it is associated with the hybridization process from the unbound state to the fully bound state.

The relaxation process associated each timescale can be determined by analyzing the eigenvector associated with that timescale. Each eigenvector is a solution up to a constant, so we rescale the eigenvector such that the largest magnitude element is 1. In this long timescale eigenvector, we see five elements with significant weight and these elements are listed in Table I. Based on these weights, we see this is not a pure transition between the unbound state and fully bound state but rather there is significant probability of transitioning to an almost bound state. The sum for all the elements in the eigenvector is equal zero. An interpretation of these elements is the change in probability that occurs for this process. We see almost 50% of the weight is in the fully bound state and 85% of the weight is in the top 4 states.

We calculated the free energy change of this process to compare to experimental results. First we determine the equilibrium probability of the states of the system from the first eigenvector of the transition probability matrix. From the equilibrium population, we calculate the change

in free energy from the unhybridized state using

$$\Delta G_i = -k_B T \ln \left(\frac{\pi_i}{\pi_1} \right), \quad (14)$$

where π_i is the equilibrium population of state i and π_1 is the equilibrium population of the unbound state. The unbound state and fully hybridized state have relatively low free energy. In order to bind, there is a free energy barrier to make first contact. This is due to a decrease in entropy in going from two free strands to one complex. This jump in free energy is concentration dependent, and a more dilute simulation would have a larger free energy jump due to a larger decrease in entropy. As binding progresses, free energy goes down until the free energy minimum which is the fully bound state. Other low free energy states are frayed states in which one or two bases from the ends of the strands are unbound. We can use this plot to calculate the free energy of binding each base pair. In Figure 3 the black line is the line of best fit of the states that appear in the 20 most likely paths. By measuring the slope of the line, we get the free energy change per base pair of $1.4 k_B T$ (0.83 kcal/mol). This is smaller than previous experimental values of about 2 kcal/mol³⁵⁻⁴⁰ but matches previous oxDNA2 results^{22,41}.

In addition to the change in free energy of hybridization, we calculate the rate of hybridization to compare to previous experimental and oxDNA results. We use three ways to calculate the rate of hybridization: the longest timescale (Equation 7), the mean first passage time (Equation 11), and from the flux (Equation 13). Using equations 7, 11, and 13 we find an agreement of $t_{\text{hyb}} = 1.8 \mu\text{s}$ for the system to hybridize. The bimolecular rate constant of our system is $k_{\text{hyb}} = ([\text{DNA}]t_{\text{hyb}})^{-1} = 1.6 \times 10^8 \text{ M}^{-1}\text{s}^{-1}$. This is slower than Ouldrige et al.²³ who found a value of $7.7 \times 10^8 \text{ M}^{-1}\text{s}^{-1}$ but still 100 times faster than experimental results⁹.

In our simulations, we visit $M = 8942$ unique states. Assuming each base can bind with any other base, and each base can only bind once, there are

$$\sum_{k=0}^N \frac{(N!)^2}{k!((N-k)!)^2} \quad (15)$$

possible states, where N is the number of bases. For $N = 14$, there are 1.6×10^{13} theoretical states. This shows that the actual number of states visited during hybridization is much smaller than the number of all theoretically possible states.

We used TPT to calculate path properties including the most likely paths, fraction visited and committor. The flux is the amount of expected transitions over time from one state to another state. From the flux we calculated the most likely paths that the hybridization took. These paths tend to be on the outer edge of our graph which indicated a zipping up pattern as seen in Figure 4. These paths do not show bases binding in a simple one-by-one matter. The two strands can make multiple hydrogen bonds within one timestep. In addition, once

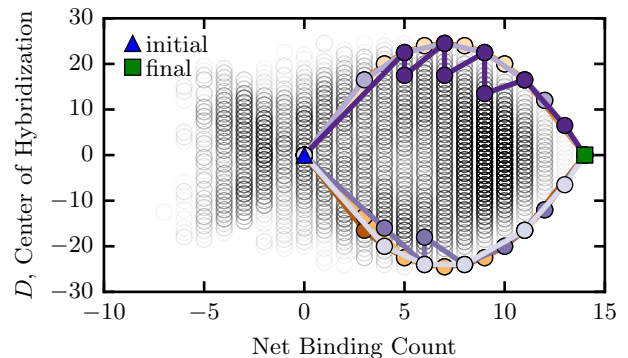


FIG. 4. Eight most likely paths that connect the unbound state (triangle) to the completely hybridized state (square), shown on a two-dimensional projection of all states onto the net binding count C and the center of hybridization D .

a base binds, it does not always stay bound through the whole mechanism. In Figure 4 we see some steps that are a vertical line. Those steps are indicative of the base at the edge unbinding, while a base towards the middle creates a new hydrogen bond.

The most likely paths show the hybridization mechanism is a zipping up pattern but the strands can also take steps that are backwards. To determine which states are important for hybridization, we calculated the fraction visited of each state. The fraction visited is the fraction of time the system will pass through a state when going from the unbound state to the bound state. States with a larger fraction visited are more important to the process. The most visited states lie along the outer edge of the plot similar to Figure 4. The outermost points in Figure 5 represent states that contain native base pairs that start from the edge of strands. The second layer of points represent states that contain only native base pairs, but the base closest to the end of the strand remains unbound. This plot also shows that the system rarely begins binding from the middle and instead it prefers to bind from the edges.

The committor is the probability of reaching a state A before reaching a state B. This is similar to a reaction coordinate in which state A is the unbound state and state B is the fully bound state in our system. The committor is considered a perfect reaction coordinate because it exactly maps to the extent of the reaction. It is not an observable however, which means it is difficult to predict the committor of a state from its coordinates. We chose Net Binding Count as a reaction coordinate because it seemed like the extent of the hydrogen bonding should be a physical and intuitive reaction coordinate. However, it is not a good reaction coordinate because it does not have a single committor for each value of Net Binding Count. In contrast, if you have a Net Binding Count of 0, you can have a committor anywhere from 0 to 1 (Figure 6). So just knowing the Net Binding Count,

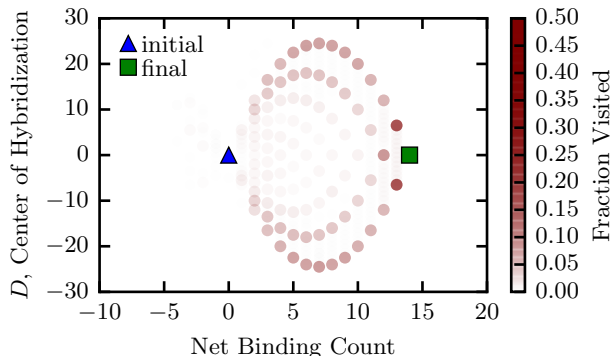


FIG. 5. Illustration of the fraction visited of states along the hybridization pathways. States that are visited more often are shown in darker colors. Multiple nested pathways are discernible, each corresponding to a zipper mechanism. The outer layer contains states with adjacent bases bound, starting with from either end of the strand. The next layer contains states in which base pairing starts at the second base from either end.

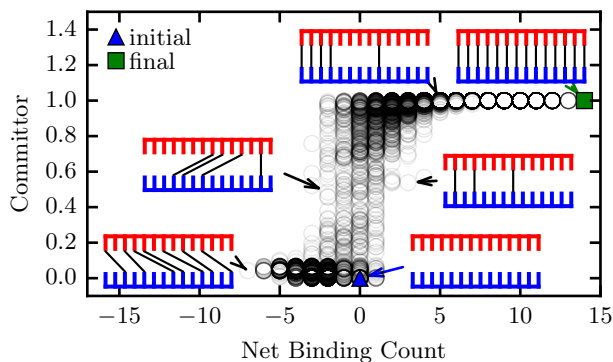


FIG. 6. Committor values of each state, projected onto the net binding count. Higher opacity indicates a larger number of states. The committor, a measure of progress towards the hybridized product state, increases rapidly at small values of C . States with the same net binding count can have very different committor values.

one can not make a good prediction of the likelihood of hybridization.

The Net Binding Count works better as a reaction coordinate for a subset of states. If we restrict the states to only those with no misaligned hydrogen bonds (only native), then the committor distribution for each value of Net Binding Count improves. For instance, without this restriction, the committor at a Net Binding Count of 1 ranges from 0 to 1, and with the restriction, the committors are between 0.2 and 0.6 (Figure 7). This restriction is limiting as it only includes 4805 states of of 8952 total states observed during the simulations.

States with a committor $0.45 < q < 0.55$ were considered transition states. In our model, there were 46

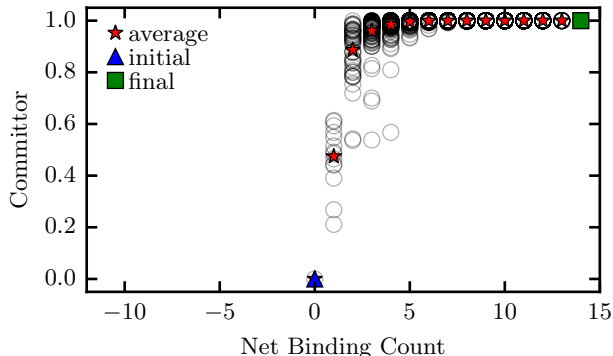


FIG. 7. Committor values of the subset of states that have only native base pairs. Considering those states only, the average committor for states with a single, native base pair is 0.5.

states with this property out of the 8952 states we observed in our simulations. To differentiate between the importance of these states we used the fraction visited. Fraction visited of an intermediate state I is the probability of going from state A to state B while passing through state I . The top 2 most visited transition states contain two natively bound bases at either end (Figure 8). These are each visited over 5% of the time. The next highest are 5 states, each with a single native base pair. These states are visited between 0.4% and 2.5%. The next most likely transition states are configurations with non-native base pairing. These states are much less likely to be visited with a fraction visited of only 0.006% or less. In general, the fraction visited value for any single state is low because the MSM can make multiple hydrogen bonds within one timestep, and the individual state may be skipped over as the system hybridizes.

To determine which states are important for the initial base pairing, we calculated which bases were most likely to be first contact bases, as well as the committor of states with only one native base pair. The transition probabilities from the unbound state determine where the first contact occurs. To determine which bases may be important first contact points, we weighted the states according to

$$f_{\alpha i} = \frac{\sum_{s=1}^M T_{1s} h_{\alpha i}(s)}{\sum_{s=1}^M T_{1s} - T_{11}}.$$

We observe first contact to be most common near the ends of the strands but not at the very end (Figure 9). The committor of states with one native base pair are shown in Figure 10. In Figure 10 we see two peaks occurring between the strand end and the strand center. This shows that the bases that have the highest probability of reaching the full hybridized state occur between

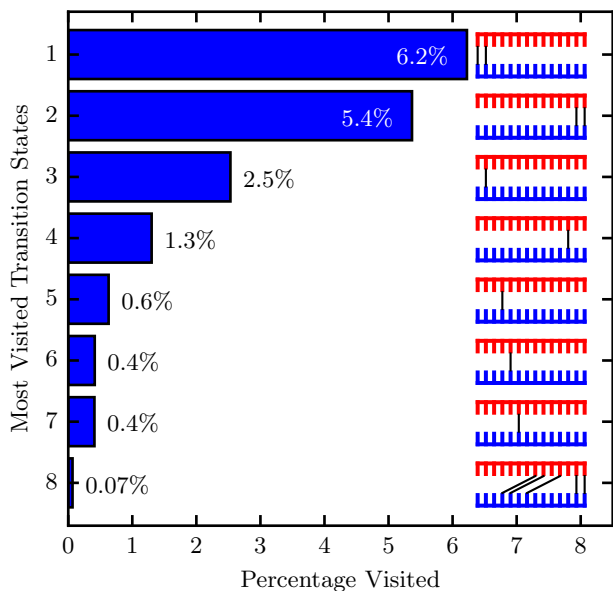


FIG. 8. The fraction visited of transition states, i.e., states with committor values between 0.45 and 0.55. Transition states with native base pairs at the ends are often visited along the hybridization pathway.

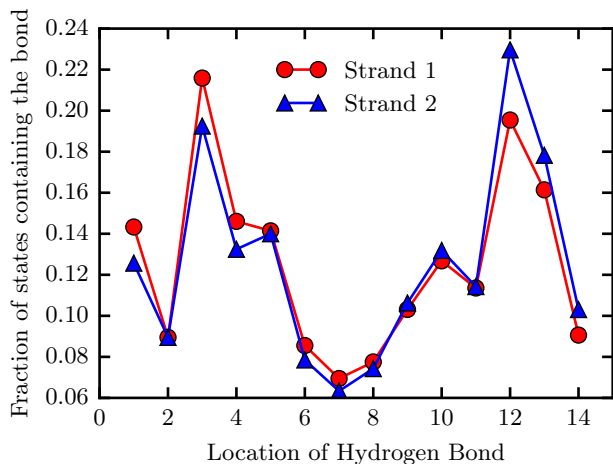


FIG. 9. Probability that a base will appear in a first contact of the two strands. We find that the third base from either end has a significantly higher probability to participate in the initial base pairing than a base in the middle or at the end of a strand.

the strand end and the strand center.

DISCUSSION

We investigated how DNA hybridizes and identified the important states and pathways in going from ssDNA to dsDNA. We identified the important states and path-

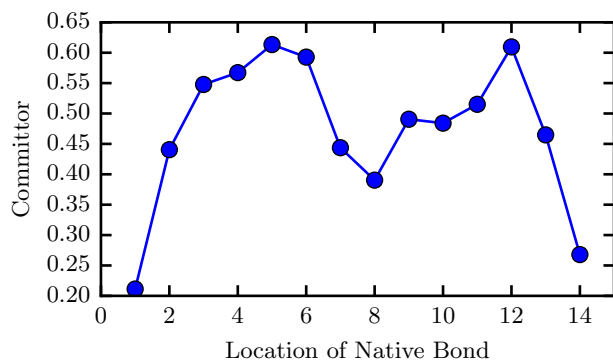


FIG. 10. The committor of states that contain only a single native base pair and no non-native base pairs. If the single base pair is at the end or in the middle then the committor is low, indicating that this nascent duplex is more likely to fall apart than to proceed to full hybridization.

ways by simulating coarse-grained DNA and creating an MSM from the simulation data. Our results suggest the most important transition states contain one or two native basepairs. To have a high likelihood of binding, we only required 3 native base pairs. Our most important pathways also show a zipping up process as suggested by previous work^{5,6}. Our results suggest that once a few bases are bound, DNA is likely to finish binding fully. The DNA tended to bind from one end instead of in the middle (Figure 5). That suggests the identity of the bases on the ends could control the kinetics more than those in the middle. The number of bases required before full hybridization in our model seems to be smaller than in other experiments^{6,7}, but is consistent with results in previous oxDNA2 simulations²³.

One strength of our approach was building up a model from simulation data. From this, we were able to get information on the large number of potential paths and the kinetics associated with those paths. By the nature of this problem, there is a large state space of theoretically 1.6×10^{13} states but we only access 8952 states. This shows the number of relevant states for hybridization is much smaller than the theoretical number of possible states.

Hybridization has been studied using oxDNA2 but using forward flux sampling, a technique for accelerating dynamics²³. Our results are consistent with those found by Ouldridge and coworkers²³. Qualitatively, they find a larger probability of initial binding near the ends of the strands. Additionally they find the probability of reaching the fully hybridized state is larger for base pairs near the middle of the strand in comparison towards the ends. They also observe a nucleation and zipping process.

Because the MSM is built from oxDNA simulations it can at best be as accurate as this coarse-grained force field. Any deficiency in the underlying force field will propagate into the MSM. Other coarse-grained models of

DNA are available, for example the 3SPN force field^{42–44}. Previously it was found that oxDNA and 3SPN exhibit different hybridization pathways²³. Not surprisingly, our MSM is consistent with previous studies of the oxDNA force field.

Another factor that limits the analysis is the choice of variable of interest. We partitioned the states by hydrogen bonding and that does not seem to be an appropriate reaction coordinate. In a good reaction coordinate, each value on the reaction coordinate should have a single value of a committor⁴⁵. This property is not seen in our committor plot (Figure 6). For instance at a Net Binding Count of 0, we have committors that range from 0 to 1. So while extent of hydrogen bonding is a physical and intuitive reaction coordinate, it is not a good reaction coordinate. It does seem to be valid for states that only contain native base pairs (Figure 7).

Creating an MSM has an important advantage over some other enhanced sampling techniques such as Umbrella Sampling⁴⁶, Metadynamics⁴⁷, or Forward Flux Sampling⁴⁸. In those methods one must first define a coordinate of interest, often called collective variable (CV), before running the simulation. However, it is often not clear beforehand which CV provides a good description of the process of interest, and one would have to perform another set of simulations if one wanted to consider different CVs. In our approach there is no need to specify a proposed CV before collecting simulation data. The MSM itself does not describe the system dynamics in terms of a one-dimensional reaction coordinate. Instead it views the dynamics as a sequence of transition in an arbitrarily complex network of states. Where we did make a choice is in the construction of the MSM when we picked a state decomposition based on the pattern of inter-strand hydrogen bonds. Making a different choice would require the calculation of another MSM transition matrix, but it would not require a new set of molecular mechanics simulations which would be computationally expensive.

CONCLUSION

We have shown that the combination of coarse-grained Brownian dynamics simulations, Markov State Models, and Transition Path Theory forms a powerful tool to study the kinetic properties and dynamical pathways of DNA hybridization. Our results are consistent with the classical zipper model: once an initial nucleus of hybridized base pairs is formed, it grows and neighboring bases zip up sequentially. We find the size of the initial nucleus to lie between one and two base pairs, and that in general the net number of base pairs is not a sufficiently informative observable to characterize the transition state ensemble.

ACKNOWLEDGMENTS

This work was facilitated through the use of advanced computational, storage, and networking infrastructure provided by the Hyak supercomputer system at the University of Washington

- ¹N. C. Seeman, *J. Theor. Biol.* **99**, 237 (1982).
- ²P. W. K. Rothmund, *Nature* **440**, 297 (2006).
- ³C. A. Mirkin, R. L. Letsinger, R. C. Mucic, and J. J. Storhoff, *Nature* **382**, 607 (1996).
- ⁴L. Y. T. Chou, K. Zagorovsky, and W. C. W. Chan, *Nat. Nanotechnol.* **9**, 148 (2014).
- ⁵J. G. Wetmur and N. Davidson, *J. Mol. Biol.* **31**, 349 (1968).
- ⁶D. Pörschke and M. Eigen, *J. Mol. Biol.* **62**, 361 (1971).
- ⁷I. I. Cisse, H. Kim, and T. Ha, *Nat. Struct. Mol. Biol.* **19**, 623 (2012).
- ⁸G. Niranjani and R. Murugan, *PLoS ONE* **11**, e0153172 (2016).
- ⁹K. M. Parkhurst and L. J. Parkhurst, *Biochemistry* **34**, 285 (1995).
- ¹⁰X. Wang, H. J. Lim, and A. Son, *Environ. Health Toxicol.* **29**, e2014007 (2014).
- ¹¹A. Barhouni and N. J. Halas, *J. Am. Chem. Soc.* **132**, 12792 (2010).
- ¹²T. G. Drummond, M. G. Hill, and J. K. Barton, *Nat. Biotechnol.* **21**, 1192 (2003).
- ¹³S. Sorgenfrei, C.-y. Chiu, R. L. Gonzalez, Y.-J. Yu, P. Kim, C. Nuckolls, and K. L. Shepard, *Nat. Nanotechnol.* **6**, 126 (2011).
- ¹⁴J. Liphardt, B. Onoa, S. B. Smith, I. Tinoco, and C. Bustamante, *Science* **292**, 733 (2001).
- ¹⁵M. T. Woodside, P. C. Anthony, W. M. Behnke-Parks, K. Larizadeh, D. Herschlag, and S. M. Block, *Science* **314**, 1001 (2006).
- ¹⁶C. Chen, W. Wang, Z. Wang, F. Wei, and X. S. Zhao, *Nucleic Acids Res.* **35**, 2875 (2007).
- ¹⁷V. V. Didenko, *BioTechniques* **31**, 1106 (2001).
- ¹⁸X. Chen, Y. Zhou, P. Qu, and X. S. Zhao, *J. Am. Chem. Soc.* **130**, 16947 (2008).
- ¹⁹G. Altan-Bonnet, A. Libchaber, and O. Krichevsky, *Phys. Rev. Lett.* **90**, 138101 (2003).
- ²⁰S. Weiss, *Science* **283**, 1676 (1999).
- ²¹J. SantaLucia and D. Hicks, *Annu. Rev. Biophys. Biomol. Struct.* **33**, 415 (2004).
- ²²B. E. K. Snodin, F. Randisi, M. Mosayebi, P. Šulc, J. S. Schreck, F. Romano, T. E. Ouldrige, R. Tsukanov, E. Nir, A. A. Louis, and J. P. K. Doye, *J. Chem. Phys.* **142**, 234901 (2015).
- ²³T. E. Ouldrige, P. Šulc, F. Romano, J. P. K. Doye, and A. A. Louis, *Nucleic Acids Res.* **41**, 8886 (2013).
- ²⁴N. Srinivas, T. E. Ouldrige, P. Šulc, J. M. Schaeffer, B. Yurke, A. A. Louis, J. P. K. Doye, and E. Winfree, *Nucleic Acids Res.* **41**, 10641 (2013).
- ²⁵G. R. Bowman, K. A. Beauchamp, G. Boxer, and V. S. Pande, *J. Chem. Phys.* **131**, 124101 (2009).
- ²⁶F. Noé, C. Schütte, E. Vanden-Eijnden, L. Reich, and T. R. Weikl, *Proc. Natl. Acad. Sci. U. S. A.* **106**, 19011 (2009).
- ²⁷V. A. Voelz, G. R. Bowman, K. Beauchamp, and V. S. Pande, *J. Am. Chem. Soc.* **132**, 1526 (2010).
- ²⁸V. S. Pande, K. Beauchamp, and G. R. Bowman, *Methods* **52**, 99 (2010).
- ²⁹P. Metzner, C. Schütte, and E. Vanden-Eijnden, *Multiscale Model. Simul.* **7**, 1192 (2009).
- ³⁰K. A. Beauchamp, G. R. Bowman, T. J. Lane, L. Maibaum, I. S. Haque, and V. S. Pande, *J. Chem. Theory Comput.* **7**, 3412 (2011).
- ³¹J. H. Prinz, H. Wu, M. Sarich, B. Keller, M. Senne, M. Held, J. D. Chodera, C. Schütte, and F. Noé, *J. Chem. Phys.* **134**, 174105 (2011).
- ³²W. E and E. Vanden-Eijnden, *J. Stat. Phys.* **123**, 503 (2006).
- ³³E. W. Dijkstra, *Numer. Math.* **1**, 269 (1959).

- ³⁴A. Dickson and C. L. Brooks, *J. Chem. Theory Comput.* **8**, 3044 (2012).
- ³⁵D. H. Turner, N. Sugimoto, R. Kierzek, and S. D. Dreiker, *J. Am. Chem. Soc.* **109**, 3783 (1987).
- ³⁶F. H. Martin, M. M. Castro, F. Aboul-ela, and I. Tinoco, *Nucleic Acids Res.* **13**, 8927 (1985).
- ³⁷F. Aboul-ela, D. Koh, I. Tinoco, and F. H. Martin, *Nucleic Acids Res.* **13**, 4811 (1985).
- ³⁸S. M. Freier, R. Kierzek, J. A. Jaeger, N. Sugimoto, M. H. Caruthers, T. Neilson, and D. H. Turner, *Proc. Natl. Acad. Sci. U. S. A.* **83**, 9373 (1986).
- ³⁹Y. Kawase, S. Iwai, H. Inoue, K. Miura, and E. Ohtsuka, *Nucleic Acids Res.* **14**, 7727 (1986).
- ⁴⁰B. L. Gaffney, L. A. Marky, and R. A. Jones, *Tetrahedron* **40**, 3 (1984).
- ⁴¹T. E. Ouldridge, A. A. Louis, and J. P. K. Doye, *J. Chem. Phys.* **134**, 085101 (2011).
- ⁴²E. J. Sambriski, D. C. Schwartz, and J. J. de Pablo, *Proc. Natl. Acad. Sci. U. S. A.* **106**, 18125 (2009).
- ⁴³D. M. Hinckley, G. S. Freeman, J. K. Whitmer, and J. J. de Pablo, *J. Chem. Phys.* **139**, 144903 (2013).
- ⁴⁴D. M. Hinckley, J. P. Lequieu, and J. J. de Pablo, *J. Chem. Phys.* **141**, 035102 (2014).
- ⁴⁵B. Peters and B. L. Trout, *J. Chem. Phys.* **125**, 054108 (2006).
- ⁴⁶G. Torrie and J. Valleau, *J. Comput. Phys.* **23**, 187 (1977).
- ⁴⁷A. Laio and M. Parrinello, *Proc. Natl. Acad. Sci. U. S. A.* **99**, 12562 (2002).
- ⁴⁸R. J. Allen, C. Valeriani, and P. Rein ten Wolde, *J. Phys.: Condens. Matter* **21**, 463102 (2009).